Compact Remnant Constraints on the Core-Collapse Engine

Chris L. Fryer

Center for Theoretical Astrophysics, Los Alamos National Laboratory, Los Alamos, NM,
87545, USA
The George Washington University, Washington, DC 20052, USA
email: fryer@lanl.gov

Abstract. The convection-enhanced neutrino-driven supernova engine's success in explaining a myriad of supernova properties has set it as the standard engine behind supernova. However, due to the success of rotationally-powered engines in explaining astrophysical transients like gamma-ray bursts, these engines have been revived as possible drivers of normal supernovae, competing with this standard engine. In this paper, these competing engines, and the constraints placed by compact remnant observations on these engines, are reviewed. We find that, with these constraints, such rotationally-powered engines can explain less than 1% of the current supernova remnants. In addition, we find that the remnant mass distribution can be used to constrain properties of the convection-enhanced neutrino-driven engine, helping astronomers understand the nature of convection in this engine.

Keywords. supernovae: general, stars: neutron, black hole physics

---

1. Competing Engines for Astrophysical Transients

Time-domain astronomy continues to discover new astrophysical transients, producing an ever-growing menagerie of transient phenomena. Despite this growing list of astrophysical explosions, four primary engines have been proposed to produce most of the transients observed in astronomy:

(1) **Thermonuclear explosions.** The energy in these models arises from the nuclear fusion of elements either in a star: in a CO white dwarf for type Ia supernovae, in pair-capture induced collapse leading to runaway nuclear burning in a pair-instability supernova, or in nuclear burning of accreting material in an X-ray burst.

(2) **Internal energy from gravitational collapse.** Mediated by neutrinos and convection, internal energy produced as gravitational energy released from the collapse of a massive star provides the energy for most type Ib/c and type II supernovae.

(3) **Accretion disk energy.** Typically mediated by magnetic fields, jets and/or viscous-driven winds drive outflows in accreting systems producing a variety of transients including X-ray binaries, gamma-ray bursts, hypernovae and, perhaps, other asymmetric supernovae.

(4) **Magnetized neutron stars.** Rotational energy in neutron stars (NS) can be tapped by magnetic fields driving pulsar and magnetar emission, soft gamma-ray repeaters and, possibly, fast radio bursts. This engine has also been proposed as an engine for supernovae and gamma-ray bursts.

The latter three all derive their energy from the potential energy released in the formation or evolution of compact objects. All three have also been proposed as engines behind at least some fraction of core-collapse (type Ib/c, II) supernovae. The key difference in these engines lies in how the gravitational potential energy released in the collapse is converted into an explosion. For example, in internal-energy engine (model *b*), the dominate engine behind core-collapse supernovae, gravitational potential energy is converted first into kinetic energy and then, through shocks, converted into internal energy. This engine is typically named after the way the internal energy is converted to explosion energy: the convection-enhanced neutrino-driven engine. Shortened names include the convective engine or the neutrin-driven engine. The accretion disk engine (model *c*) and the pulsar/magnetar engine (model *d*) both convert the gravitational potential energy into rotational kinetic energy and then use this rotational energy to power their transients.

In this paper, we focus on these three engines and their role in explaining core-collapse supernovae. By comparing the predictions from these different engines to the properties of observed compact remnants, we can constrain both the rate and properties of these engines. It is important to note that all of these engines likely produce some of the observed transients in astrophysics. Our focus is instead on their efficacy in producing normal core-collapse supernovae. In section 2, we review the mechanisms behind the engines when used to explain core-collapse supernovae. In section 3, we review the observed properties of compact remnants both before and after the recent observations from gravitational waves. In this section, we also review the current limitations of these observations. In section 4, we apply the constraints to our different engines to determine rates and characteristics of these engines. We conclude with a discussion of additional observations that have also guided the nature of the supernova engine.

2. Overview of the Engines

All our proposed engines for supernovae begin the same: the collapse of the core of a massive star. A massive star undergoes a series of nuclear burning phases, fusing the ashes from the previous burning phase to form heavier elements. This burning occurs in both the core and different layers of the star as the inner star compresses and heats. The core of a massive star is supported by electron degeneracy and thermal pressures. In stars above $\sim 8\,M_\odot$, the core becomes so dense and hot that electrons capture onto protons (producing neutrons and electron neutrinos). With the loss of electron degeneracy pressure, the stellar core implodes (Fig. 1). The collapse continues until the core reaches nuclear densities where neutron degeneracy pressure and nuclear forces halt the collapse, sending a bounce shock through the star and forming a proto-NS that will ultimately cool to form a 10 km NS. But this bounce shock stalls without producing an explosion.

This is where the engines diverge. The collapse released an immense amount of gravitational potential energy. During the bounce much of this energy is converted into thermal energy. It is this thermal energy that the convective engine will tap to drive an explosion. If the core is rotating, a fraction of the gravitational energy is converted into rotational kinetic energy. The magnetar mechanism taps the rotational energy in the collapsed core (proto-NS). The accretion disk mechanism taps the rotational energy in a disk surrounding the compact object. Let's study these engine mechanism in more detail.

2.1. *Convective Supernova Engine*

The convection-enhanced neutrino-driven engine behind core-collapse supernovae is the current standard paradigm for normal supernovae. During the bounce, most of the gravitational potential energy is converted into internal energy in the proto-NS core. The core is so hot and dense that this energy primarily is emitted through neutrinos.
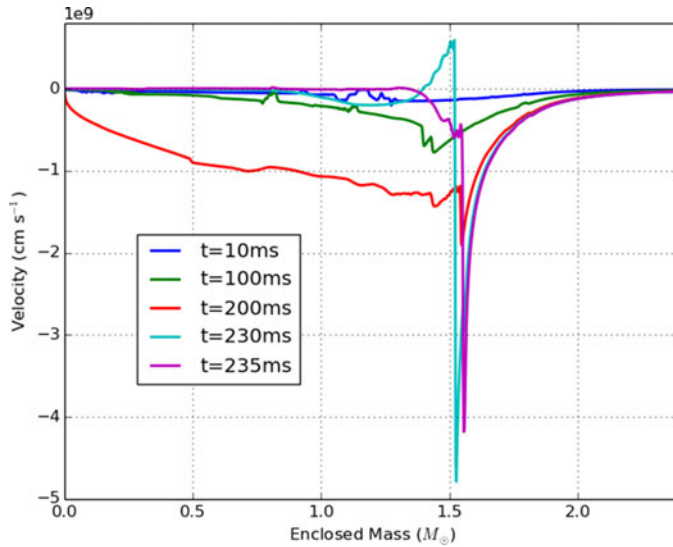
Figure 1. Velocity profiles (velocity versus radius) at 5 different times in the collapse and bounce of a $15\,M_\odot$ model from Fryer et al. (2018). Electron capture initiates the collapse and quickly becomes a runaway process as the higher collapsed densities accelerate the capture rate. When the core reaches nuclear densities (roughly 230 ms after the start of this calculate), the core bounces driving a bounce shock outward that stalls roughly 5 ms later. Although this explosion fails, it sets up the conditions (entropy gradient) to initiate convection that later helps to drive this explosion.

Tapping 1% of this neutrino emission is sufficient to drive and explosion. However, the simple neutrino driven mechanism did not work alone. Fortunately, the stalled bounce shock leaves behind a region that is unstable to convection and this convection can enhance the efficiency of this neutrino-driven explosive engine.

One of the advantages of this standard paradigm is that it has been studied in great detail and the multi-dimensional physics has been modeled for nearly 3 decades with increasingly sophisticated physics. Figure 2 shows a slice of a 3-dimensional simulation of stellar collapse after the development of convection in the region between the proto-NS and the stalled shock. This convection aids the neutrino-driven mechanism two ways. First, the neutrinos emitted from the proto-NS deposit their energy primarily at its surface. Convection allows that heated material to rise, converting this thermal energy into kinetic energy that pushes against the infalling stellar material to drive an explosion. Second, convection reduces the pressure of the infalling material by allowing it to, instead of piling up at the position of the stalled shock, flow down to the proto-NS, releasing more potential energy to drive an explosion. Figure 2 shows both of these aspects of the convection-enhanced engine: the upward rising bubbles generating kinetic energy and the downflows reducing the pressure of the imploding star.

This mechanism provided a natural explanation for the observed $0.5 - 2 \times 10^{51}$ erg supernova energies. Until then, it was not understood well how the collapse, which releases 10^{53} erg of energy could produce explosions of only 10^{51} erg. The convective engine proceeds until it can overcome the infalling material from the imploding star. In the first 1 s of the collapse (before the accretion of the infalling material causes the core to collapse to a black hole), the energy needed to overcome the ram pressure of the imploding star is $0.5 - 2 \times 10^{51}$ erg[For more details, see Fryer et al. (2021)]. As we shall discuss in section 5, the convection also matched well the structures in the supernova ejecta.
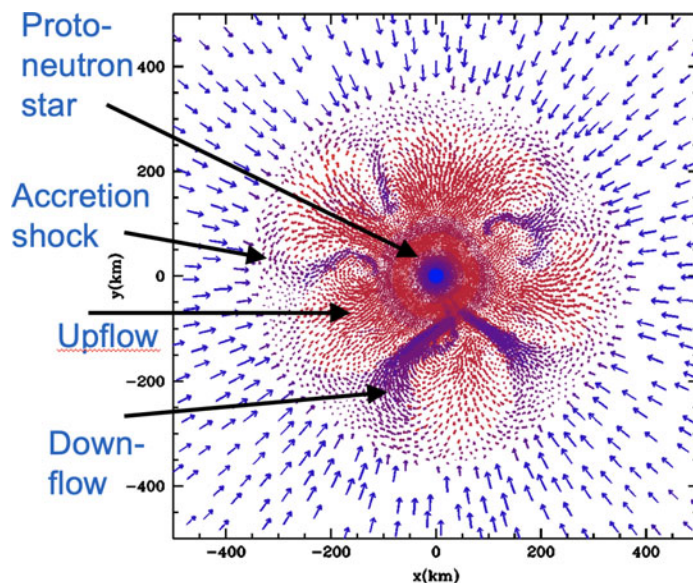
Figure 2. Slice of a 3-dimensional simulation of stellar collapse after the development of convection between the proto-NS and the stalled shock. Convection aids the explosion in two ways: 1) material heated by neutrinos near the surface of the NS is able to expand, converted the neutrino energy into kinetic energy exploding the star and 2) infalling material from the star does not pile up on the surface, but flows down to the proto-NS releasing additional potential energy.

This engine identified 3 different compact remnant formation scenarios tied to the explosion strength: strong supernova explosions and NS formation, weak explosions and black hole formation through fallback, and no explosions and massive black hole formation (Figure 3). Fallback plays a key role in determining this mass and, although the physics to determine this fallback is simpler and can be studied[Fryer (2006)], many remnant studies do not include it.

The simple picture behind Fryer (1999) and Fryer & Kalogera (2001) predicted a smooth distribution of NS and BH remnant masses. But it was later realized that the growth time of the convection in this engine produced a range of results [Fryer et al. (2012), Belczynski et al. (2012)]. By studying a range of convective growth times, Fryer et al. (submitted to ApJ) found that observed distributions of the remnant masses provided insight into this convective growth time (Figure 4). The shape of the curves fitting remnant masses versus the CO core mass depend on this growth time because faster convection allows the energy to increase in the convective region more quickly, driving an explosion when the ram pressure is still high. The resultant stronger explosion-energy has less fallback, leading to a more narrow region where weak explosions exist. This produces fewer fallback BH systems and a shift in the BH mass distribution.

2.2. *Accretion Disk Engines*

Accretion disk engines gained notoriety after the success of the collapsar engine in explaining long-duration gamma-ray bursts [Woosley (1993)]. This model argues that some of the material in a rapidly-rotating star would have sufficient angular momentum to hang up in a disk around the collapsed core. Magnetic fields could wind up in this disk to create a magnetically-driven jet that produces the observed gamma-ray burst properties. But the angular momentum needed to form such a disk is non-trivial. The
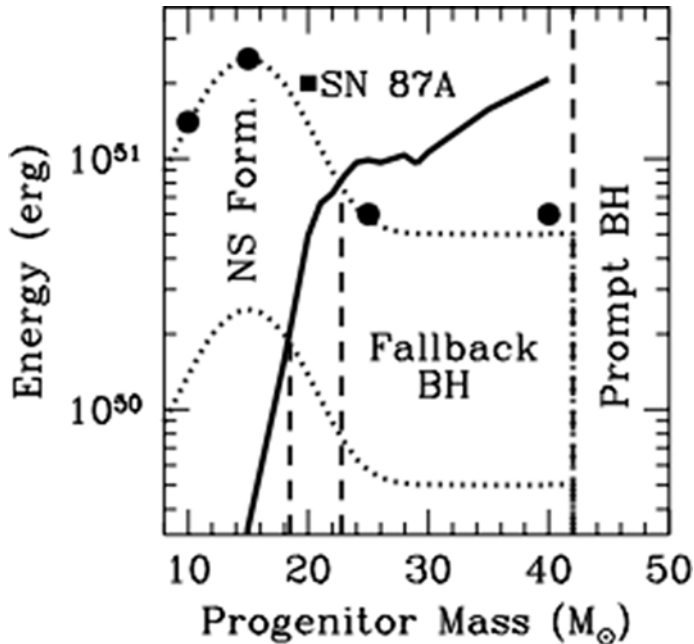
Figure 3. Explosion energy versus progenitor mass. The dots show the results from 2-dimensional simulations from Fryer (1999). The solid curve shows the binding energy of the star beyond the inner $3 M_\odot$. The dotted curves are rough estimates of the expected explosion energy based on fits to the simulations from Fryer & Kalogera (2001). Comparing the binding energy to the explosion energy, the 3 stellar fates could be easily seen. With explosions where the explosion energy was much higher than the binding energy, very little material falls back after the launch of the explosion. As the binding energy increases, the energy also decreases leading to the weak explosion/high fallback scenario. Finally, there are models where convection is unable to revive the shock. After 1-10 s of accretion, the core collapses to a black hole.

specific angular momentum (j) needed to form a 100 km disk around a newly collapsed compact object is given by:

$$j = 4 \times 10^{14}(M_{\rm rem}/1.4 M_\odot)\,{\rm cm}^2{\rm s}^{-1} \qquad (2.1)$$

where $M_{\rm rem}$ is the remnant mass. Figure 5 shows the angular momentum profile of a set of rotating stars along with the angular momentum required to form a disk. These are some of the most optimistic stellar models (born rotating at near-maximum rotation speeds). Even in such scenarios, when the star expands to the giant phase, its spin rate decreases dramatically. If the core is coupled to this expanded envelope, it would be spinning too slowly at collapse to form a disk. Only the models that completely decouple the core from the outer layers have enough angular momentum to produce a disk around a low-mass remnant. Even modest coupling (expected in stellar models) produces stars that can produce a disk only after considerable mass has accreted onto the compact remnant. Gamma-ray burst modelers have spent nearly two decades devising different progenitor systems with sufficient angular momentum to produce these disks [Fryer et al. (1999)].

Because the angular momentum increases in the outer layers of the star, gamma-ray burst theorists focused on building disks around black holes (allowing the accretion of low-angular momentum material onto the black hole). But this did not stop scientists from invoking a similar accretion disk model around NSs for normal supernovae [Akiyama et al. (2003)]. At this time, no realistic progenitor model at the time had sufficient angular
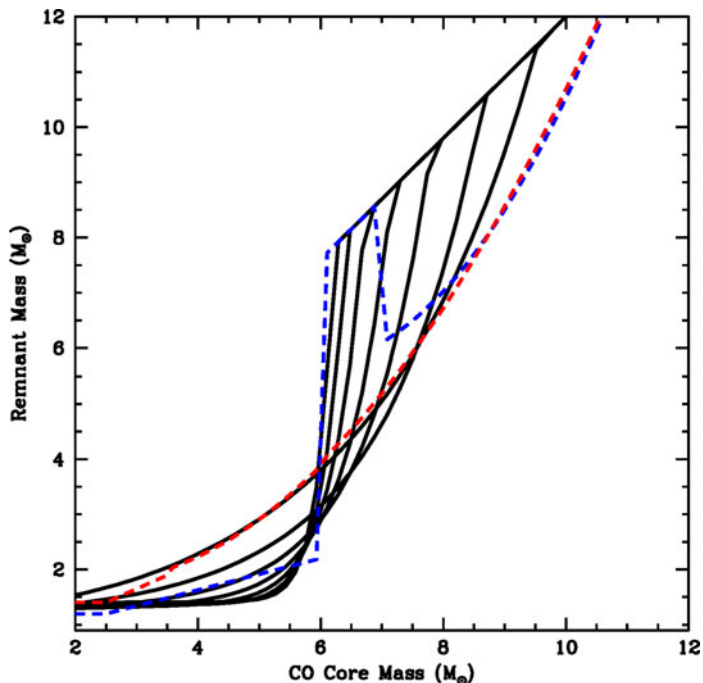
Figure 4. Remnant mass versus CO core mass for both the models used by Fryer et al. (2012) and Belczynski et al. (2012) and the parameterized growth-time models of Fryer et al. (submitted to ApJ). The faster the convective growth time, the more sharp the transition between strong and no explosion. This produces a gap between NS and BH formation.

momentum to make a disk around a NS during a stellar collapse [Fryer & Warren (2004)], the most likely would be the merger of two compact cores [Fryer & Heger (2005)]. This has not stopped the community from producing artificial progenitors that are rotating rapidly enough to form an accretion disk [Mösta et al. (2018)].

Recent stellar models argue for very strong coupling between stellar layers, meaning that the spin rate of the core slows down immensely in the giant phase [Fuller & Ma (2019),Fuller et al. (2019)]. With such cores, no disks (either around NSs are BHs) are possible. The only way to produce fast-rotating cores in this scenario is either to spin up the compact object through asymmetric mass ejection in a supernova (NS cases), through stellar mergers causing the spin up or through tidal locking in close binaries. In the tidal-locking scenario, Fryer et al. (submitted to ApJ) found that no disks would form around NSs and only 1% of BH-forming systems would form disks (possibly sufficient to explain long-duration gamma-ray bursts).

Perhaps stellar evolution models are incorrect. Perhaps there is some binary mechanism that spins stars more rapidly than tidal-locked estimates predict. Remnant observations will help us determine whether the NS accretion disk mechanism can work or whether it is just possible in artificial theory models.

2.3. *Magnetar Engines*

Magnetars are the engine behind both anomalous X-ray pulsars/soft gamma-ray repeaters [for a review, see Mereghetti et al. (2015)]. In addition, in binary NS mergers, rotation rates are sufficiently high to power gamma-ray bursts and, more-importantly, the X-ray plateaus in short-duration gamma-ray bursts [Mereghetti et al. (2015)]. But
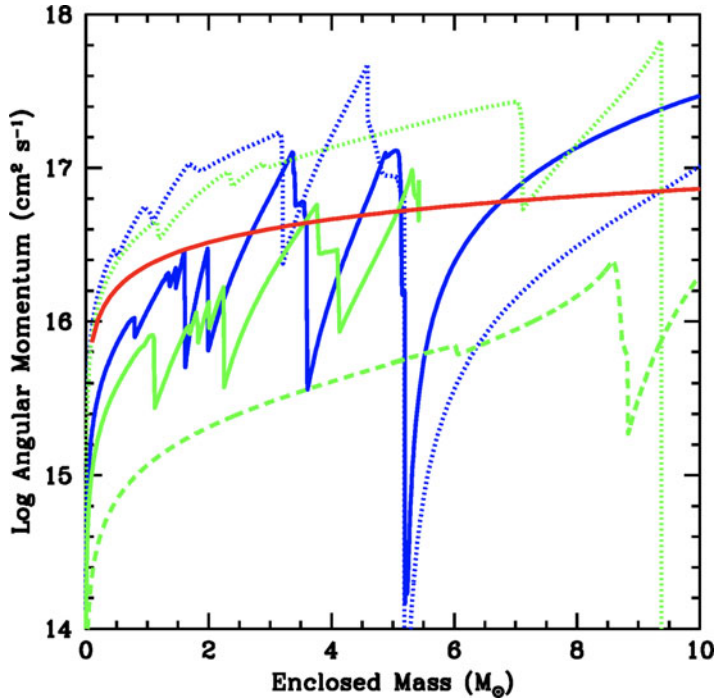
Figure 5. Angular momentum profile (specific angular momentum versus of enclosed mass) for two different stellar models: $15\,M_\odot$(blue), $25\,M_\odot$ (green). The dotted lines correspond to models using the *GENEC* code with no magnetic dynamo [Belczynski et al. (2020)], the solid lines correspond to models using the Kepler code using a weak magnetic dynamo Heger et al. (2005), and the dashed line corresponds to simulation using a stronger magnetic dynamo using the *MESA* code [Paxton et al. (2013)]. The solid red line corresponds to the angular momentum needed to make a 1000 km disk around the compact remnant (Fig. 1 from Fryer et al. (2019)).

in stellar collapse, these engines have the same difficulties with models invoking accretion disks: getting enough angular momentum. Here we review the angular momentum requirements for this engine based on energy requirements. The moment of inertia of a NS (I_{NS}) is given by:

$$I_{NS} = 10^{45}(M_{NS}/M_\odot)\text{g cm}^2 \qquad (2.2)$$

where M_{NS} is the NS mass. The corresponding rotational energy (E_{rot}) is:

$$E_{rot} = 1/2 I_{NS}\omega^2 = 5 \times 10^{50}(\omega/1000 Hz)^2 \text{ erg} \qquad (2.3)$$

where ω is the angular velocity. If the NS is spinning with a 1 ms period, it can produce a 10^{51} erg explosion if it can tap 10% of the rotational energy to drive an outflow. However, bear in mind that if magnetars are to be the engine driving the supernova explosion, we can not use the spin period once it has become a compact 10 km NS. The proto-NS is 30 km in size and, for a proto-NS that will become a 1 ms magnetar, the spin at 30 km requires 100% energy-extraction efficiency to produce an explosion with a normal supernova explosion energy.

This argues that magnetar engines are better suited as *additional* power sources to a supernova explosion. For instance, a 100 ms magnetar tapping 10% of its rotational energy after collapse can produce a 10^{47} erg power source that, if converted directly to thermal energy, can explain the luminosity of a super-luminous supernova. But this

requires that the supernova explosion itself (the blast that ejects the star) be powered by another engine (presumably the convective engine).

The other difficulty in using magnetars to power supernovae is that it is difficult to achieve the magnetic fields required at the early times during formation [for a review, see Mereghetti et al. (2015)]. Two mechanisms have been proposed: fossil magnetic fields and dynamo-generated magnetic fields. If the magnetic fields are in the collapsing star, the magnetic fields will couple to the infalling material, sapping the rotational energy of NS prior to its final collapse. In addition, most progenitor stars do not have the strong fossil magnetic fields to produce magnetar-like fields [Keane & Kramer (2008),Woods (2008)]. Alternatively, magnetic fields can develop through dynamo action in the proto-NS[Duncan & Thompson (1992)]. Typically, this dynamo occurs at late times, growing over 1-10s [Keil et al. (1996)]. If the supernova doesn't launch in the first second, the core will collapse to a black hole, so this model requires an explosion prior to magnetic-field generation. With current understanding of the magnetic field generation, magnetar fields are likely produced after the launch of a supernova (presumably from the convective engine).

As with the NS accretion disk mechanism, perhaps we are missing some critical aspect in our model, e.g. the correct magnetic-field generation mechanism. Again, the clues might lie in the compact remnant observations.

3. Properties of Compact Remnants

We have reviewed the different engines behind core-collapse supernovae and their requirements. Let us now compare them to the observed properties of compact remnants. Because some of the insight from gravitational wave observations differed from that of other observational constraints, we will divide this section into two subsections describing compact remnant properties before and after gravitational wave detections.

3.1. *Prior to Gravitational Waves*

Observations of binaries containing NSs and BHs (e.g., X-ray binaries and binary pulsars) have placed strong constraints on their mass distributions. Observations of close pulsar binary systems where extremely accurate masses can be obtained through pulsar timing dominated initial estimates of the mass distribution of NSs. Originally, analyses of these binaries suggested a very narrow mass distribution around $1.35\,M_\odot$ [Thorsett & Chakrabarty (1999)]. More recently, as available data have increased and became more refined, it has become clear that the mass distribution has some spread which better fit the predictions of the convective engine. In many cases, these new observations and analyses argued for a bimodal distribution [Antoniadis et al. (2016),Farr & Chatziioannou (2020)]. With evidence of NS masses as low as $1.1\,M_\odot$ [Lattimer (2019)] and a succession of newly observed massive NSs with masses near or above $2\,M_\odot$ has demonstrated the width of this distribution whether it is bimodal or fit by some other distribution: PSRs J1614−2230 [Demorest et al. (2010)], J0348+0432 [Antoniadis et al. (2013)], and J0740+6620 [Cromartie et al. (2020)]. Despite the ever-widening distribution, there remains strong evidence that there is a gap in remnant masses between 2.5 and $4\,M_\odot$ [Farr et al. (2011),Altamirano et al. (2011)]. As we shall see in section 4, these mass constraints provide vital information into the convective engine.

Pulsar observations also have the potential to estimate the distribution of birth spin periods of NSs. However, to do so, astronomers must account for the spin-down of these NSs through pulsar emission. By assuming a model for spin-down and estimating the age of the pulsars, astronomers can calculate the birth spin period. The fastest pulsars could be born spinning with spin-periods less than 10 ms (the Crab pulsar is believed to have

been born spinning at 17 ms). Popov & Turolla (2012) found that a Gaussian with an average spin period with an average of 100 ms (with a $1 - \sigma$ deviation of 100 ms) fits the observations. Faucher-Giguère & Kaspi (2006) found a slightly higher average of 300 ms ($1 - \sigma$ deviation of 150 ms). Igoshev & Popov (2013) argue that the differences between these two studies could be explained by the choice of magnetic field evolution and either distribution could be made consistent with the data. Noutsos et al. (2013) also obtained a distribution of periods peaking below 125 ms, but found an additional set of long-period birth spins (> 0.5 s). They found that poor age estimates limit determinations of the birth pulsar spin distribution and described methods to estimate pulsar ages kinematically.

Although the observed NS spin distribution is fairly low, the BH systems observed through X-rays argue for high-angular momentum progenitors. For example, the BHs in wind-fed high mass X-ray binaries (HMXB) for which we have spin estimates all suggest that the progenitors produce black holes near the maximum spin values. The estimated spins of these BHs can be described in terms of dimensionless spin parameter: $a_{\mathrm{spin}} = (cJ_{\mathrm{BH}})/(GM_{\mathrm{BH}}^2)$ where c is the speed of light, G is the gravitational constant and J_{BH} and M_{BH} are the total angular momentum and mass of the black hole respectively. The current calculated a_{spin} values of the observed X-ray binary black holes are: $a_{\mathrm{spin}} = 0.92$ for LMC X-1, $a_{\mathrm{spin}} = 0.983$ for Cyg X-1, $a_{\mathrm{spin}} = 0.84$ for M33 X-7. If these spin values represent the birth spins of most black holes, this suggests that there is very little coupling between burning layers within a star. Such rapidly spinning stars would form ms pulsars. But it is worth remembering that these spin estimates are difficult to determine [for a review, see Belczynski et al. (2021)]. BH spins can be measured by two methods: disk reflection and disk continuum. For LMC-1 and Cyg X-1 BH spins from both methods are consistent, while for M33 X-7 BH spin was estimated only through disk continuum [Miller & Miller (2015)].

In summary, prior to gravitational wave predictions, NS and BH observations: a) argued for a gap in the $\sim 2.5 - 4\, M_\odot$ region between NS and BH formation and b) NS observations argued for modest and BHs argued for high spin-rates of stars.

3.2. *Gravitational Wave Constraints*

The discrepancies in these measurements, combined with the uncertainties and biases in their measurements, require additional diagnostics. Gravitational wave astronomy, still in its infancy, has already placed strong constraints on both the mass and spin distributions of compact remnants [for a review, see The LIGO Scientific Collaboration et al. (2021)].

The LIGO sample still is limited by the sample size allowing some wiggle room in the constraints on compact remnant populations, but a few basic discovers alter our intution from before gravitational-wave studies:

• **NS/BH mass gap:** Already, studies of remnant masses fromg gravitational waves have altered the notion of a NS/BH mass gap. Current observations suggest that remnants do exist in this region. As more data is collected, we will be able to determine whether this region is part of a smooth distribution, or more likely, ther is more of a dip in the masses between $2.5 - 4.0\, M_\odot$. In any event, the gap is less pristine than it was first thought.

• **BH spins:** Gravitational waves measure do not measure the spin, but a quantity $\chi_{\mathrm{eff}} = (M_{\mathrm{BH1}} a_{\mathrm{spin1}} cos\theta_1 + M_{\mathrm{BH2}} a_{\mathrm{spin2}} cos\theta_2)(M_{\mathrm{BH1}} + M_{\mathrm{BH2}})$ where $M_{\mathrm{BH1,2}}$, $a_{\mathrm{spin1,2}}$ are the masses (1,2) and spins (1,2) of the two binary components and $\theta_{1,2}$ are the respective spin axes with respect to the orbital axis. The gravitational wave distribution suggests that 90% of the observed black holes have $|\chi_{\mathrm{eff}}| < 0.2$ and their samples suggest 99% have $|\chi_{\mathrm{eff}}| < 0.4 - 0.5$.

Table 1. Rate Constraints Based on Rotational Models (% of Collapsed Systems)

Constraint	Convective	Magnetar	Disk
X-ray Binary	100?%	100?%	$< 1 - 10$?%
Pulsar ($P_0 = 100$ ms, $\sigma = 100$ ms)	100%	1%	0.3%
Pulsar ($P_0 = 300$ ms, $\sigma = 150$ ms)	100%	0.03%	0.01%
GW	100%	< 0.01%	< 0.01%

To match the observed systems, Belczynski et al. (2020) argued that most black holes must be born with very little spin ($a_{\rm spin} < 0.1$. This corresponds to tightly-coupled burning layers [e.g. Fuller & Ma (2019),Fuller et al. (2019)] with the only fast-spinning black holes arising from tidally-locked systems.

A couple interpretations could explain the differences between past results and these new LIGO results. The simplest explanation is that these observations are all detecting different populations and it could be that the different populations have different properties. Although this probably explains some differences, it is likely that some of the differences lie in uncertainties in the analyses. For example, in filling the mass gap: the mass gap was only evident when detailed statistical methods were used to interpret the existing data and, in general, the data was consistent with the mass gap. It is likely that the observed pulsar/X-ray binary data are also consistent with a mass dip, indeed some studies argued that these studies over-interpreted the results [e.g. Fryer & Kalogera (2001)]. As is often the case, if a better set of priors for the Bayesian statistical methods is used, e.g. a dip (rather than a dearth) of remnants in this region is allowed, it is likely that a "dip" solution would fit the observed data. Similarly, Belczynski et al. (2021) have argued that the uncertainties in the spin estimates from X-ray binaries may be larger than assumed and that the spin rates of the BHs in these systems may indeed be lower. It is important to realize that the gravitational wave systems also have biases (the most obvious being that gravitational waves are more sensitive to massive BHs - however, stellar models suggest that this should not bias our spin estimates) that may be misrepresenting our sample.

4. Putting it all together

As we compare our engines with the observations, we will use different observations to constrain different engines. Neither of the rotational models are currently sufficiently detailed to make strong predictions on the mass distribution. However, the stringent angular momentum requirements place strong constraints on these engines. In contrast, the convective engine is less affected by rotation but makes specific remnant-mass predictions from which we can constrain this engine.

4.1. Rotational Constraints

The current angular momentum constraints all point to the fact that our rotationally-powered models must be extremely rare. Let's discuss the constraints from different observations separately: BH X-ray binaries, pulsars, gravitational-waves (see Table 1 for a summary). It is important to note that the convective engine is not strongly effected by the rotation. Rotation tends to reduce the convection so fast-rotating models may be harder to explode [Fryer & Heger (2000)]. These explosions will have fewer upflows (and hence appear more bimodal), but this doesn't dramatically affect the explosion (and could perhaps explaining some peculiar supernovae).

X-ray Binary Constraints: If all stars produce the high spin values seen in X-ray binaries, coupling between burning layers in stars is weak. If we assume this coupling in lower-mass, NS-forming stars, these stars are all born with periods below 4.5 ms. At

4.5 ms, if the magnetar engine can tap all of the rotational energy, it can drive a 10^{51} erg explosion (but this requires a collapse down to a 10 km NS prior to the explosion). However, the angular momentum constraints to form a disk around a NS are even more extreme. Although many of the BH-forming systems in this scenario will form disks, less than 1-10% of NS-forming systems will form disks.

Pulsar Constraints: If we assume the pulsar distribution best describes the angular momentum of the stars, the fraction of rotationally-powered engines drops significantly. For example, with the pulsar distribution described by a Gaussian distribution with a peak at $P_0 = 100$ ms and a $\sigma = 100$ ms, only 1% of systems would have spin periods below 4.5 ms and less than 0.3% would form disks. A distribution with $P_0 = 300$ ms and a $\sigma = 150$ ms argues that $< 0.03\%$ of systems could be magnetar-driven and $< 0.01\%$ would have NS disks. It is worth noting that we are assuming that we are 100% efficiency at extracting energy from a 10 km NS (recall, the NS just after bounce is closer to 30 km). We have also ignored issues with developing the magnetic fields. With this data, at best, one in a hundred (and the true answer is likely to be much lower) supernovae are powered by magnetars or disks. However, these same distributions allow 0.1-3.6% of supernovae to gain 10^{50} erg from a magnetar, possibly augmenting the power behind superluminous supernovae.

Gravitational Wave Constraints: Finally, if the angular momentum constraints from the BHs observed in gravitational waves is correct, most systems are born spinning slowly. In this case, most NS-forming collapses would not have sufficient angular momentum to either produce a disk or a magnetar-powered supernova. Explaining the pulsar spin distribution would require some explosion-driven spin-up [i.e. Blondin & Mezzacappa (2007)]. Fryer et al. (submitted to ApJ) studied the role of the tidally locked systems. Although 1% of the BH-forming systems could form accretion disks, none of the NS systems would form disks or be rotating sufficiently fast to produce magnetar-powered explosions. Here again, roughly 0.1-1% of collapsing stars could augment the power of a superluminous supernova.

Based on the gravitational-wave and pulsar constraints, it appears rotationally-powered engines are ruled out for 99% of supernovae not associated with gamma-ray bursts.

4.2. *Mass Constraints*

Since rotationally-powered models do not predict mass distributions and they are unlikely to produce many of the observed remnants, we will focus our attention on the constraints placed on the convective engine from the observed mass distributions. The span of the NS and black hole mass distributions was one of the first true predictions by the convective engine. That is, when the convective paradigm first predicted [Fryer & Kalogera (2001)] a range of remnant masses, observations argued for a delta function distribution of these masses. At the time, this engine was in conflict with the existing observations. However, with time, observational constraints changed and this prediction from the model has become the more standard interpretation of the data. But this first analysis did not predict a mass gap and the existence of the mass gap poses problems for a simple convective model. The mass gap (or even a dip) can be used to place constraints on the engine.

As we discussed in section 2, the timescale for the growth of convection can alter the remnant mass predicted for a given progenitor. Fryer et al. (submitted to ApJ) developed a prescription for the final baryonic remnant mass (M_{remnant}) that allows a range of growth timescales:

$$M_{\text{remnant}} = 1.2 + 0.05 f_{\text{mix}} + 0.01 (M_{\text{CO}}/f_{\text{mix}})^2 + e^{f_{\text{mix}}(M_{\text{CO}} - M_{\text{crit}})} \qquad (4.1)$$
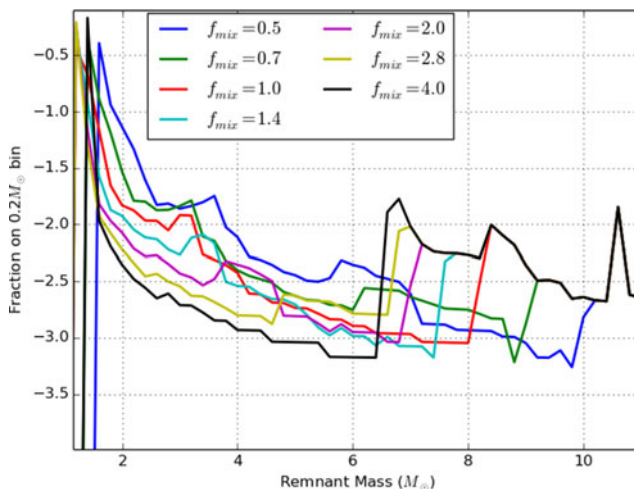
Figure 6. Distribution of baryonic compact remnant masses for seven different values of f_{mix}. The depth and width (in remnant) space depends upon this mixing growth rate. The position in mass coordinates depends on M_{crit}: this plot uses a value of $4.75\,M_{\odot}$. None of these models predict no compact remnant masses in the mass gap, but the fraction can drop by a factor of 10 between slow and fast growth times.

where M_{CO} is the Carbon/Oxygen core mass, M_{crit} is a critical mass for black hole formation (for the models shown in Figure 6, we use $M_{\mathrm{crit}} = 4.75\,M_{\odot}$) and f_{mix} is a parameter describing the mixing growth time. Figure 6 assumes a simple initial mass function for the distribution of stars, limiting the maximum remnant mass to that of the helium core. The "dip" in the masses in the gap, especially the position of this dip, can provide critical information on this convective growth time.

Of course, the distribution shown in Figure 6 can not be compared directly to observed distributions. Any prescription for compact remnant formation must then be integrated into models studying the progenitors of our observed systems. Olejak et al. (in preparation) are studying the masses expected in binary systems based on these prescriptions.

5. Additional and Future Constraints

The fact that the convective engine, the standard paradigm behind core-collapse supernova, is much more able to explain the constraints placed by compact remnant observations than rotation-powered engines does not come as a surprise to most supernova engine modelers. The convective engine has been studied by a number of teams using the fastest supercomputers in the world, studying the physics behind the engine and verifying these models. We already discussed the fact the convective engine both provided a natural explanation for the 1% efficiency in energy extraction from stellar collapse and predicted a range of remnant masses when observations argued for a set of delta function distributions. Neither of the rotationally-powered models are sufficiently developed to make such predictions and, as we have seen, tend to not have the energies to produce the observed supernova explosion. The convective engine was driven by observations of asymmetries in supernovae [for a review, see Fryer et al. (2021)], but the specific multi-outflow model predicted by convection was supported by recent observations of the supernova ejecta remnants [Grefenstette et al. (2014).Grefenstette et al. (2017)]. These models have been tested against observations of the nucleosynthetic yields and supernova light-curves.

Astrophysics tends to forget its history. Rotation has been proposed multiple times to explain the engines behind supernovae and, every time, against the observations of the time, it has always provided a poor fit. The fact that rotation can explain a subset of transients, e.g. systems like soft gamma-ray repeaters and gamma-ray bursts, does not mean that this engine will suddenly work for normal supernova. Observations of compact remnants, especially their constraints on rotation, have firmly proven that magnetars or NS accretion disks can not power normal supernovae. At best, they are important for rare events or adding power to normal explosive engines. This does not mean they are not important engines to explain different phenomena in the broad menagerie of astrophysical transients. But each engine has its place.

Upcoming observations will not only place rigid constraints on the angular momentum of stellar progenitors, but will also allow us to sufficiently understand the NS/BH gap region to place even more stringent constraints on convection in the supernova engine. One of the most powerful remnant observatories is the next generation of gravitational wave detectors [Kalogera et al. (2021)]. These detectors will see BH/BH binaries out to the edge of the universe and will build an extremely large sample of remnant masses. Equally exciting is the potential of gravitational lensing events to detect isolated compact remnants. Whereas all of our other observations focus on systems in close binaries, these lensing events have the potential to observe remnants from single-star systems, probing a new population of remnant formation. In addition, new methods and new observations of Galactic X-ray binaries and pulsar systems continue to improve the constraints from these observed systems. As we improve our binary population studies, tying remnant observations to specific evolutionary scenarios, we can use these different observations to not only study the supernova engine, but binary evolution as well.

References

The LIGO Scientific Collaboration, the Virgo Collaboration, the KAGRA Collaboration, et al. 2021, *arXiv:2111.03634*

Akiyama, S., Wheeler, J. C., Meier, D. L., et al. 2003, *ApJ*, 584, 954

Altamirano, D., Belloni, T., Linares, M., et al. 2011, *ApJL*, 742, L17

Antoniadis, J., Freire, P. C. C., Wex, N., et al. 2013, *Science*, 340, 448

Antoniadis, J., Tauris, T. M., Ozel, F., et al. 2016, *arXiv:1605.01665*

Belczynski, K., Wiktorowicz, G., Fryer, C. L., et al. 2012, *ApJ*, 757, 91

Belczynski, K., Klencki, J., Fields, C. E., et al. 2020, *A&A*, 636, 104

Belczynski, K., Done, C., & Lasota, J.-P. 2021, *arXiv:2111.09401*

Blondin, J. M. & Mezzacappa, A. 2007, *Nature*, 445, 58

Cromartie, H. T., Fonseca, E., Ransom, S. M., et al. 2020, *Nature Astronomy*, 4, 72

Demorest, P. B., Pennucci, T., Ransom, S. M., et al. 2010, *Nature*, 467, 1081

Duncan, R. C. & Thompson, C. 1992, *ApJL*, 392, L9.

Farr, W. M., Sravan, N., Cantrell, A., et al. 2011, *ApJ*, 741, 103

Farr, W. M. & Chatziioannou, K. 2020, *Research Notes of the American Astronomical Society*, 4, 65

Faucher-Giguère, C.-A. & Kaspi, V. M. 2006, *ApJ*, 643, 332

Fryer, C. L., Woosley, S. E., & Hartmann, D. H. 1999, *ApJ*, 526, 152.

Fryer, C. L. 1999, *ApJ*, 522, 413

Fryer, C. L. & Heger, A. 2000, *ApJ*, 541, 1033

Fryer, C. L. & Kalogera, V. 2001, *ApJ*, 554, 548

Fryer, C. L. & Warren, M. S. 2004, *ApJ*, 601, 391

Fryer, C. L. & Heger, A. 2005, *ApJ*, 623, 302

Fryer, C. L. 2006, *New Astronomy*, 50, 492

Fryer, C. L., Belczynski, K., Wiktorowicz, G., et al. 2012, *ApJ*, 749, 91

Fryer, C. L., Andrews, S., Even, W., et al. 2018, *ApJ*, 856, 63

Fryer, C. L., Lloyd-Ronning, N., Wollaeger, R., et al. 2019, *European Physical Journal A*, 55, 132

Fryer, C. L., Karpov, P., & Livescu, D. 2021, *Astronomy Reports*, 65, 937

Fuller, J. & Ma, L. 2019, *ApJL*, 881, L1

Fuller, J., Piro, A. L., & Jermyn, A. S. 2019, *MNRAS*, 485, 3661

Grefenstette, B. W., Harrison, F. A., Boggs, S. E., et al. 2014, *Nature*, 506, 339

Grefenstette, B. W., Fryer, C. L., Harrison, F. A., et al. 2017, *ApJ*, 834, 19

Heger, A., Woosley, S. E., & Spruit, H. C. 2005, *ApJ*, 626, 350

Igoshev, A. P. & Popov, S. B. 2013, *MNRAS*, 432, 967

Kalogera, V., Sathyaprakash, B. S., Bailes, M., et al. 2021, *arXiv:2111.06990*

Keane, E. F. & Kramer, M. 2008, *MNRAS*, 391, 2009

Keil, W., Janka, H.-T., & Mueller, E. 1996, *ApJL*, 473, L111

Lattimer, J. M. 2019, *Universe*, 5, 159

Mereghetti, S., Pons, J. A., & Melatos, A. 2015, *Space Science Review*, 191, 315

Miller, M. C. & Miller, J. M. 2015, *Physics Reports*, 548, 1.

Mösta, P., Roberts, L. F., Halevi, G., et al. 2018, *ApJ*, 864, 171

Noutsos, A., Schnitzeler, D. H. F. M., Keane, E. F., et al. 2013, *MNRAS*, 430, 2281

Paxton, B., Cantiello, M., Arras, P., et al. 2013, *ApJS*, 208, 4

Popov, S. B. & Turolla, R. 2012, *Astrophysics and Space Sciences*, 341, 457

Strang, L. C. & Melatos, A. 2019, *MNRAS*, 487, 5010

Thorsett, S. E. & Chakrabarty, D. 1999, *ApJ*, 512, 288

Woods, P. M. 2008, *40 Years of Pulsars: Millisecond Pulsars, Magnetars and More*, 983, 227

Woosley, S. E. 1993, *ApJ*, 405, 273.